

# Dynamic Mechanical Properties of Spherical Inclusions in Polymer Composite: A Self-Consistent Approach Considering Morphology

M. SHATERZADEH,<sup>(1)</sup> C. GAUTHIER,<sup>(1)</sup> J. F. GERARD,<sup>(2)</sup> C. MAI,<sup>(1)</sup>  
and J. PEREZ<sup>(1)</sup>

<sup>(1)</sup>Laboratoire du Groupe d'Etudes de Métallurgie Physique et de Physique des Matériaux (G.E.M.P.P.M.)  
UMR 5510, C.N.R.S., INSA de Lyon  
F-69621 Villeurbanne Cedex, France

<sup>(2)</sup>Laboratoire des Matériaux Macromoléculaires (L.M.M.)  
UMR 5627, C.N.R.S., INSA de Lyon  
F-69621 Villeurbanne Cedex, France

In this work, the dynamic mechanical behavior of epoxy/A-glass bead composites is investigated considering the influence of the volume fraction of the beads and their surface treatments. The main differences between the different samples are observed in the rubbery modulus plateau. The "Self-Consistent Scheme" is used to calculate the effective shear modulus of the composite with spherical inclusions, i.e., a macroscopically isotropic polymer medium containing spheres. The 3-phase model first introduced by Christensen and Lo accurately predicts results for the composite with treated glass beads (sizing agent), but fails for the other one (untreated surface). For the latter composite, other related models (4-phase models) are also applied without satisfactory results. Then, the 3-phase model is applied in successive steps to account for the specific distribution of glass.

## 1. INTRODUCTION

Particulate reinforced materials are often used as model systems for the interpretation of the mechanical behavior of composites in which the filler is of more complex geometry (1-2). The general scheme consists in comparing experimental results with theoretical predictions in order to understand the effect of each component, i.e. the filler, the matrix, and the interface. In the case of polymer matrix, the comparison is generally based on dynamic mechanical properties. Actually, it is generally admitted that the harmonic response of a linear viscoelastic body, subjected to oscillating boundary stress, can be predicted by replacing modulus terms in the static linear elastic solution with the corresponding complex viscoelastic modulus at fixed frequency. This is generally referred to as the elastic-viscoelastic correspondence principle (3). Thus, the developments of micromechanical models based on spherical composite inclusions are now widely used, and applied to predict the dynamic mechanical response of reinforced polymers. Models can be divided into three types: (i) Phenomenological macroscopic analysis, such as Takayanagi (4); (ii) Variational mod-

els, e.g., Hashin and Shtrikman (5); and (iii) Self-Consistent Scheme, e.g., Hill (6), and Budiansky (7). In the latter type, different formulations with more or less sophisticated approximation degrees have been proposed since Kerner's formulation (8) referred to 3-phase models (9), 4-phase models (10, 11), and  $(n+1)$  phase models (12).

However, some discrepancies between theoretical predictions and experimental results are still often observed. Several explanations have been given. One explanation is the dependence on temperature of the properties of the components: the Poisson's coefficient (13, 14) and shear modulus (15). For a polymer such as epoxy, the Poisson's coefficient in the glassy state is around 0.32, while it increases toward 0.5 in the rubbery state. Since the temperature dependence of  $G_f$  and  $G'_m$  (resp. the storage shear modulus of filler and of the matrix) are not the same, the magnitude of the ratio  $G'_f/G'_m$  increases slightly with temperature below the main mechanical relaxation and much more through it and above. A second important point is the state of dispersion of the inclusions at the mesoscopic scale (1, 2, 16). Actually, if the distribu-

tion is not homogeneous, some regions can display nearly close packed spheres (i.e. aggregates), whereas other parts of the composite material have lower volume fractions of spheres. Actually, it is found in the literature that the formation of strong aggregates increases the shear modulus the same as viscosity is increased by aggregation.

In this paper, we analyze the dynamic mechanical behavior of composites with a crosslinked matrix (epoxy) reinforced with spherical A-glass particles with several filler contents or surface treatments. Experimental dynamic mechanical experiments were carried out using a low frequency torsion pendulum operating in forced oscillations. After a brief survey of the micromechanics approaches, the complex shear modulus of the composite is calculated using the classical 3-phase and 4-phase models. When the distribution of the fillers appears to be nonhomogeneous, the classic models fail to fit the data. Then, a new method based on the repeated application of the 3-phase Self-Consistent Scheme (SCS) is proposed. This method allows us to introduce the nonuniform arrangement of the reinforcing phase in the material and yields to accurate prediction.

## 2. EXPERIMENTAL

### 2.1. Materials

Composite specimens based on a polyepoxy matrix reinforced with different volume fractions of A-glass beads were prepared.

The epoxy network was synthesized from an epoxy prepolymer (diglycidyl ether of bisphenol-A: DGEBA, DER 332 from Dow Chem.,  $n = 0.02$ ) and a primary diamine comonomer (isophorone diamine: IPD, from Hüls Chem.). The reaction was made in bulk with a stoichiometric ratio of amino to hydrogen-epoxy equal to one, after degassing at 60°C during 40 minutes under vacuum. The A-glass beads (from Sovitec, A05040) were added to the DGEBA/IPD mixture and the reactive system was stirred during 30 min under vacuum. The samples were prepared as 6-mm-thick plates in a PTFE-coated mold. For curing, the epoxy reactive system was cured according to the following cure schedule (17):

- i: from room temperature to 413 K (2K/min)
- ii: one hour at 413 K
- iii: second heating from 413 K to 463 K (2K/min)
- iv: final stay at 463 K for six hours

The average particle size of the A-glass spheres was 40  $\mu\text{m}$ . Different volume fractions of A-glass beads were introduced in the polymer, ranging from 0% (neat matrix) to 50%. Glass beads were used with untreated surfaces or treated with ( $\gamma$ APS) aminosilane.

The morphology of composites was observed in the cross section of the sample with an optical microscope (Zeiss). The observations indicate that the distribution of glass beads is less homogeneous when the surface is untreated, as illustrated in Fig. 1.

### 2.2. Dynamic Mechanical Spectroscopy (DMS)

Dynamic mechanical spectroscopy was carried out using an inverted torsion pendulum illustrated in Fig. 2. For this apparatus, the micromechanalyzer concept originates from the G.E.M.P.P.M. laboratory of INSA de Lyon and was developed by Metravib Co. This is an inverted torsion pendulum device operating in forced oscillations at very low frequencies (from  $10^{-5}$  Hz to 1 Hz). This apparatus allows the investigation of the dynamic mechanical behavior of materials, such as the storage shear modulus,  $G'$ , and the loss modulus,  $G''$ , and the internal friction  $\tan \delta = G''/G'$  (loss tangent) as a function of temperature (for one or several frequencies) or frequency (under isothermal conditions) (18).

Parallelepipedic specimens ( $55 \times 6 \times 2$  mm<sup>3</sup>) were milled from the molded plates for these experiments. Measurements were performed from 100 K to 464 K in a frequency  $F = 1$  Hz.

## 3. EXPERIMENTAL RESULTS

Figure 3 shows the experimental plots of  $\log G'$ ,  $\log G''$  and  $\log \tan \delta$  versus temperature from 100 K to 500 K at a fixed frequency (1 Hz) for the neat matrix and the composites filled with various volume fractions of untreated glass beads (from 0% to 50%). The  $\tan \delta$  spectra display the two well-known relaxations of the epoxy networks: (i) the  $\alpha$  main peak associated with the glass transition region and located at 446K, (ii) the  $\beta$  relaxation peak at 240 K (secondary relaxation),

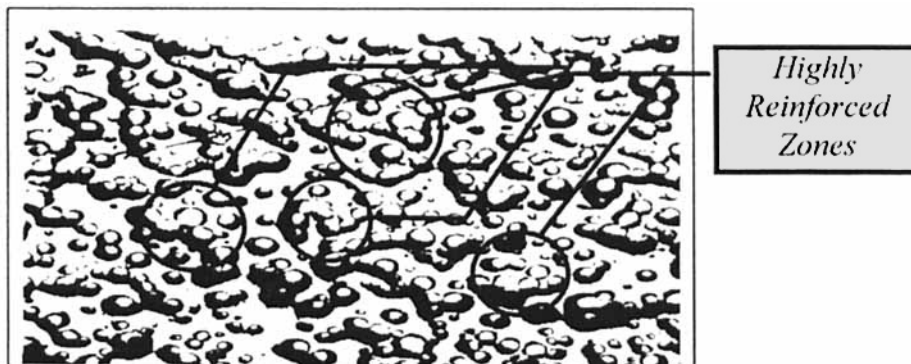


Fig. 1. Micrographic observation of the composite with untreated glass beads ( $\phi_f = 30\%$ ).

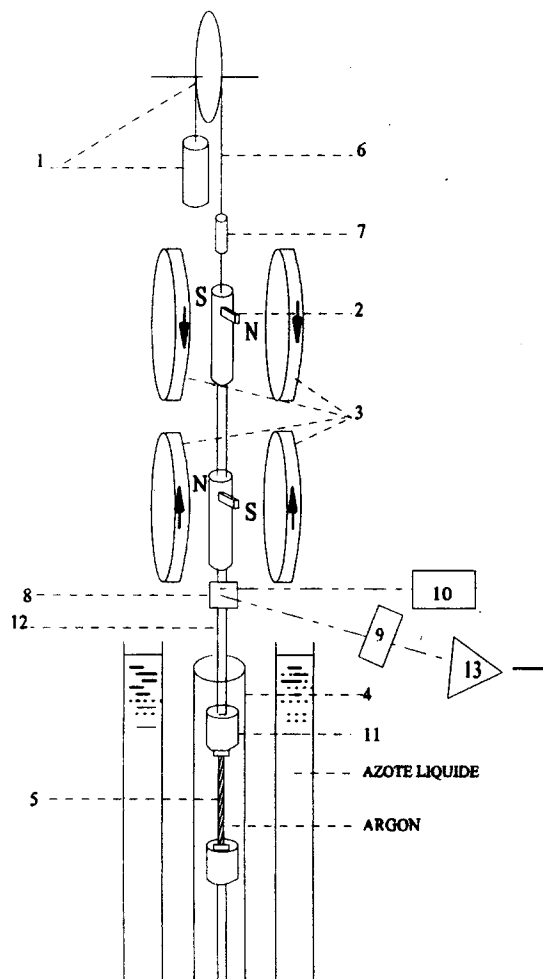


Fig. 2. Scheme of the mechanical spectrometer. (1) Pulley + counter weight; (2) Magnet; (3) Helmholtz's seals; (4) Copper oven; (5) Sample; (6) Suspension wire; (7) Damper; (8) Mirror; (9) Differential photovoltaic cell; (10) Light regulated source; (11) Moving jaw; (12) Stiff rod; (13) Low-drift amplifier.

which is considered to be associated with the motions of hydroxyether units (19). Several successive measurements were done in order to verify that no physical aging occurred during the experiments. Some of the main experimental values are reported in Table 1. These results show that with increasing volume fraction of filler,  $G'$  at 100K increases, whereas  $G'$  at 464 K is highly enhanced. In the same time, the magni-

Table 1. Comparison of Dynamic Mechanical Properties of the Neat Matrix and Composite Materials Based on Various Volume Fractions of Untreated Glass Beads (Experimental Data).

	$T_{\alpha}$ (K)	$\tan(\delta)_{\max}$	$G'$ (MPa) (at T=100K)	$G'$ (MPa) (at T=464K)
Matrix DGEBA/IPD	446	1.1	2450	10.8
Composite 10%	447	1	3050	14.3
Composite 20%	448	0.95	3700	21.4
Composite 30%	449	0.90	4450	38.9
Composite 50%	449	0.80	6750	66.6

tude of the mechanical relaxation decreases and the maximum of the peak is slightly shifted toward higher temperatures ( $\approx 3^{\circ}\text{C}$ ). Nevertheless, it has been checked by DSC measurements that the glass transition temperatures of both samples (matrix and composite) are very close. That means that no major change in the crosslinking degree of the epoxy matrix occurs in the composite, or that this change actually concerns only a very small volume near the interface.

Experimental results ( $G'$  and  $G''$ ) for composites with 30%-aminosilane treated glass beads are also presented in Fig. 4 and compared with samples containing 30%-untreated beads. We can observe that the data are very similar except for the modulus in the rubbery plateau, which appears to be higher for the composite with untreated beads. The same trends are also observed for the other amount of glass beads, when  $\phi_f > 20\%$ .

#### 4. CALCULATIONS BASED ON SELF-CONSISTENT APPROACHES

The estimation of effective properties for complex microstructures has been significantly improved, in recent years, by the use of self-consistent homogenization methods. In such an approach, the heterogeneous material, loaded on its external boundaries, is treated as a uniform medium supporting a field of fictitious volume forces. The displacement, strain, and stress fields at equilibrium are then derived using the Green tensor introduction technique (20). In the heterogeneous material, each "phase" is regarded as an inhomogeneity included in a reference uniform matrix with mean properties. In the standard self-consistent approximation, the reference matrix is assumed to display the properties of the unknown material. In the case of isotropic materials, for instance, Hashin and Shtrikman proposed to give to the matrix the bound properties of the hardest (weakest) phase of the real material (5).

As this type of approach is convenient for granular materials but not for materials with connected phases (21), specific analyses for the latter ones have been developed as, for instance, the composite sphere model of Hashin (22). The "generalized self-consistent" scheme received a first analytical formulation by Christensen and Lo in the case of 2-phase materials (9), known as the 3-phase model. In this approach, the system is described considering a spherical inclusion surrounded by a matrix shell, which in turn is surrounded by the effective equivalent medium (Fig. 5) [bounded in Mackenzie (23), and infinite in Christensen and Lo (9)]. Extensions to materials with more than two phases were later proposed from the concept of multi-layered inclusions, as, for example, the 4-phase model of Maurer (10) (introducing an inter-phase). Recently, the generalization to  $(n + 1)$ -phase model in the case of  $n$ -layered spheres has been proposed by Herve and Zaoui for isotropic elasticity (12). It can be noted that the solution developed by Herve and Zaoui, for  $n = 2$ , is similar to the 3-phase model

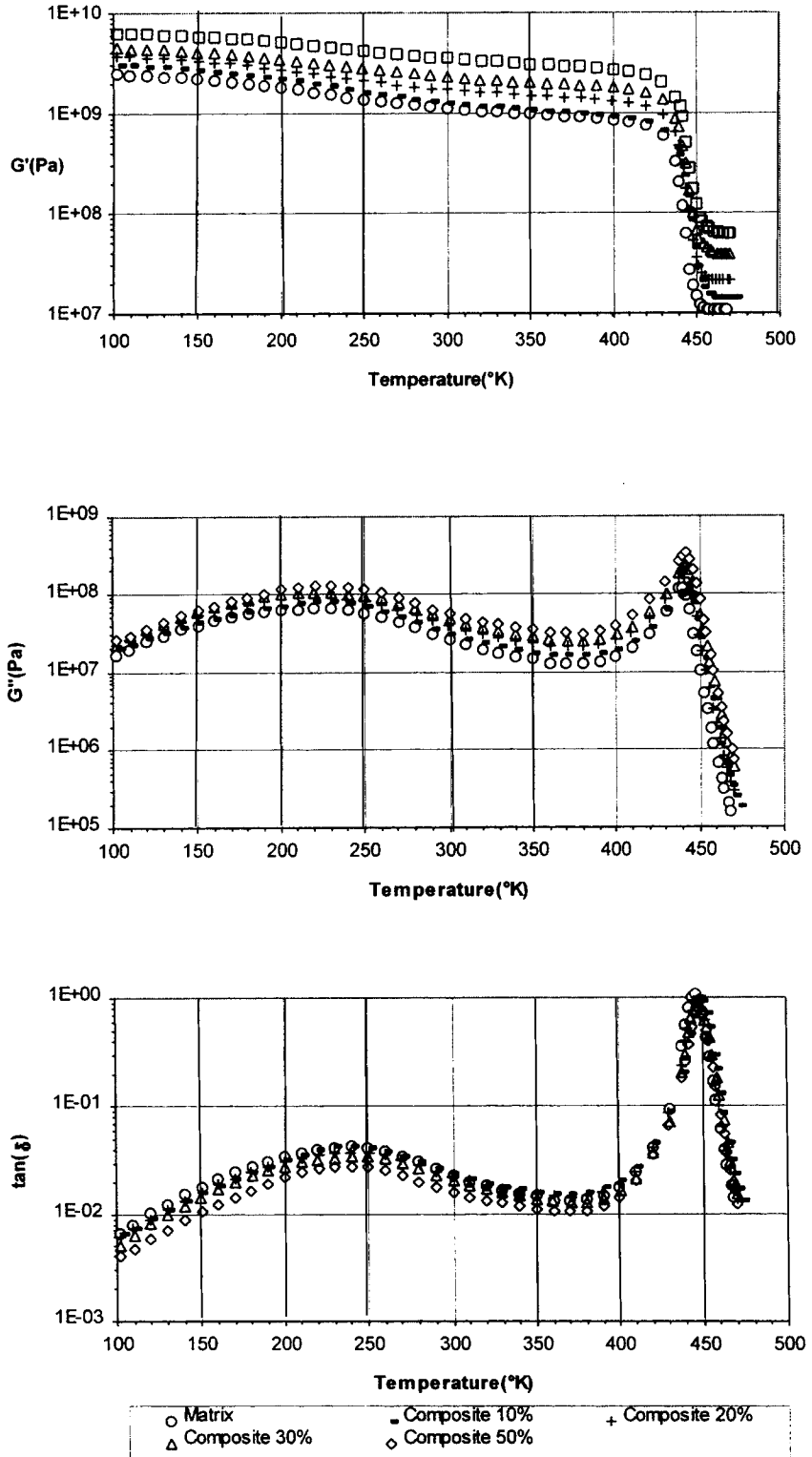


Fig. 3. Experimental spectra for the neat matrix and the composites with different volume fractions of untreated glass beads.

from Christensen and Lo (9); it will be simply called the 3-phase model in the following.

The 3-phase model consists of a single composite sphere embedded in an infinite medium (Fig. 5) of unknown effective properties. The ratio of radii in Fig. 5

is taken such that  $\frac{R_1^3}{R_2^3} = \phi_f$ , the volume fraction of the inclusion phase. In the case of a simple shear, the displacement is given in terms of spherical coordi-

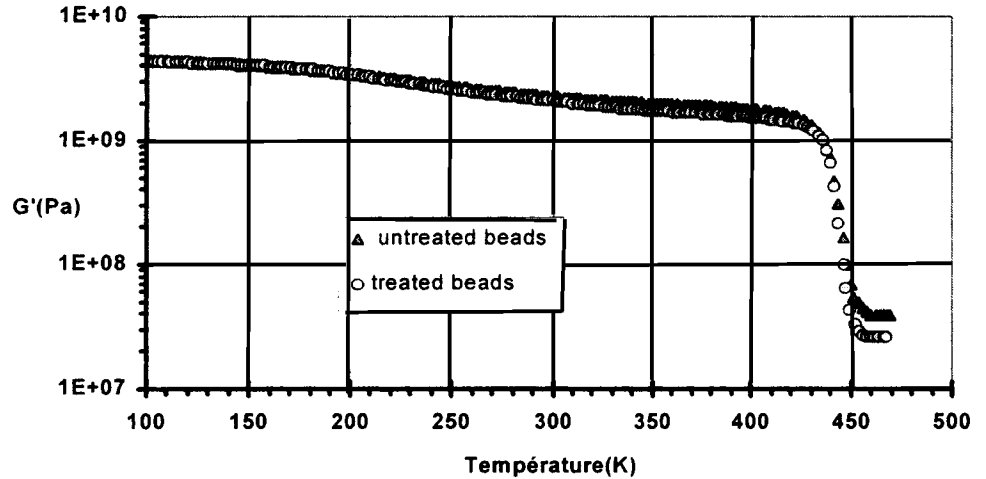
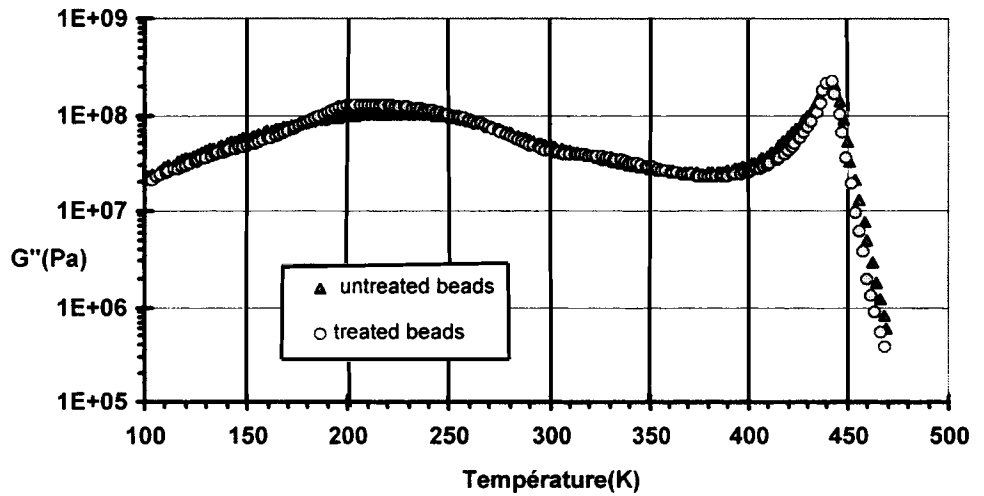


Fig. 4. Experimental spectra for the composites filled with treated and untreated glass beads ( $\phi_f = 30\%$ ).



nates  $(r, \theta, \gamma)$  according to:

$$u_r = U_r(r) \sin^2 \theta \cos 2\gamma \quad (1)$$

$$u_\theta = U_\theta(r) \sin \theta \cos \theta \cos 2\gamma \quad (2)$$

$$u_\gamma = U_\gamma(r) \sin \theta \sin 2\gamma \quad (3)$$

with 
$$U_\theta = -U_\gamma \quad (4)$$

where  $U_r$ ,  $U_\theta$ , and  $U_\gamma$  are unknown functions of  $r$  only, and these can be solved from the equilibrium equations.

By giving the general forms of the elasticity solution (24), for the three phases (Fig. 5), the equilibrium equation can be resolved as:

$$U_r^{(i)} = A_i r - 6 \frac{\nu_i}{1-2\nu_i} \cdot B_i r^3 + 3 \frac{C_i}{r^4} + \frac{5}{1-2\nu_i} \frac{4\nu_i}{r^2} \cdot \frac{D_i}{r^2} \quad (5)$$

$$U_\theta^{(i)} = A_i r - \frac{7-4\nu_i}{1-2\nu_i} \cdot B_i r^3 - 2 \frac{C_i}{r^4} + 2 \frac{D_i}{r^2} \quad (6)$$

where  $i$  is the index for the filler ( $=1$ ), matrix ( $=2$ ) and equivalent homogeneous media ( $=3$ );  $\nu_i$  is the Poisson's coefficient of each phase, and  $A_i$ ,  $B_i$ ,  $C_i$ , and  $D_i$  are constants. The constants  $C_1$ ,  $D_1$ , and  $B_3$  obviously vanish ( $r = 0$  and  $r \rightarrow \infty$ ) and  $A_3$  is determined from the boundary conditions at an infinite distance. After some calculations (10) in the case of a simple shear deformation, and by considering the passage, from elastic ( $G_c$ ) to viscoelastic ( $G_c^*$ ), (25, 26), the final equation for shear modulus of composite ( $G_c^*$ ) is given by the following second order equation:

$$X \left( \frac{G_c^*}{G_m^*} \right)^2 + Y \left( \frac{G_c^*}{G_m^*} \right) + Z = 0 \quad (7)$$

where  $X$ ,  $Y$ , and  $Z$  are constants and  $G_m^*$  is the dynamic shear modulus of matrix. The simplified expressions of the constants  $X$ ,  $Y$ , and  $Z$  for 3-phase model are given in the Appendix. Using the quadratic equation (Eq 7), the solution for the equivalent shear modulus of the spherical model can be determined.

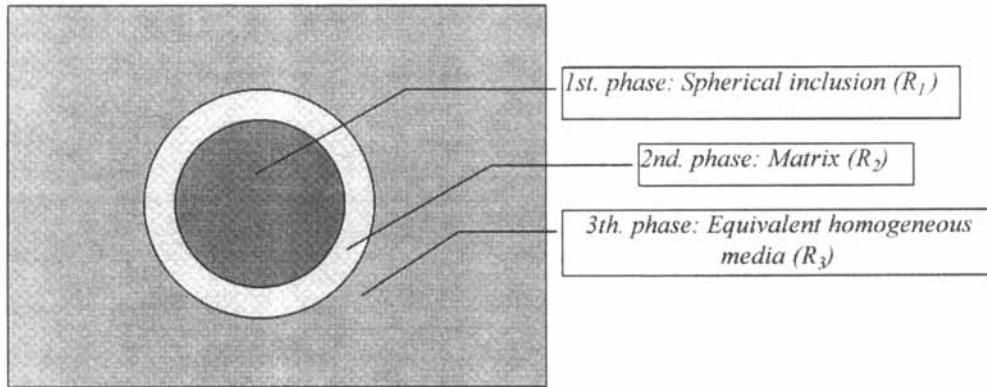


Fig. 5. Three-phase model scheme.

## 5. COMPARISON BETWEEN CALCULATIONS AND EXPERIMENTAL RESULTS

### 5.1 Application of the 3-Phase Model

Numerical results given by the 3-phase model were carried out by developing a program computed under a mathematical software (Mathcad-Plus packages). Calculations require that the behavior of each phase is available. The Poisson's coefficient,  $\nu_f$  and Young's modulus of filler,  $E_f$  are constant and equal to 0.22 and 72 Gpa, respectively.

The complex shear modulus of epoxy matrix has been determined experimentally. The Poisson's ratio of the matrix is assumed to change from 0.32 to 0.5 when the main relaxation occurs, similarly to the modulus following Equation 8:

$$\nu_{mj} = 0.32 + 0.179 \frac{\log G'_{m|T=100K} - \log G'_{m|T}}{\log G'_{m|T=100K} - \log G'_{m|T=464K}} \quad (8)$$

where  $\nu_m$  is the Poisson's coefficient of the matrix, and  $j$  the index of the temperature from 100 K to 464 K.

Figure 6 shows the calculated curves of  $G'$  versus temperature for both composite samples based on 30 vol% untreated and treated glass beads. It appears that, in the case of treated glass beads, the experimental shear modulus is fitted by the model on the whole temperature range. On the contrary, in the case of untreated beads, the rubbery modulus is underestimated.

If we consider the other volume fractions, the 3-phase model always gives a good estimation of the properties of the composites filled with treated glass beads. On the contrary, when  $\phi_f > 20\%$  of untreated glass beads, the 3-phase model cannot be used for predicting the rubbery modulus. But, for low volume fractions of untreated filler (10%), a correct fit is obtained, as illustrated on Fig. 7. We can add that, in the case of low filler content (10%), the Kerner model also gives a good estimation for both samples. Nevertheless, at larger amounts of glass beads, the calculated values given by the Kerner model are far from the experimental data in the rubbery state (see as an example the interrupted curve in Fig. 6b). That means,

once again, that the Kerner equation is adapted only for the dilute media.

As experimental data of untreated fillers are fit for low glass volume fractions and no more for higher values, one can assume that these differences arise from the morphology of the material, i.e., the spatial distribution of filler in the matrix. As already mentioned, the distribution of untreated glass beads in the epoxy matrix is not homogeneous especially when filler content increases (Fig. 1). Actually, in the 3-phase model, the description of the material assumes that the glass bead is totally and uniformly embedded in the neat resin. That point is invalidated by the nonhomogeneous distribution of the untreated fillers in the cross section of the specimen when  $\phi_f > 20\%$ . In other words, the distribution of the fillers in this material is too far from uniformity to estimate correctly the effective properties with the 3-phase model.

### 5.2 Application of the 4-Phase Model

In a second step, we decided to try other developments from the self-consistent scheme, as for example the 4-phase model. We first used the 4-phase model from Maurer (10), but no satisfactory fit was obtained. Actually, this model is devoted to a sample with an interphase. In our case, it should have been more appropriate for treated glass beads, where the chemical interactions between filler and matrix are of a chemical nature. But for the treated beads, the direct application of the 3-phase is already adequate.

Then, we also tried the model proposed by Mele and Alberola. This model seems very interesting, as it is based on the same micromechanical description (4-phase model) and claims to take into account the percolation concept. For volume fractions above the percolation threshold, the authors proposed to use a four-component scheme with (i) the matrix, which is packed in the percolated glass beads; (ii) a continuous medium of glass; (iii) a shell of the polymer matrix; and (iv) a surrounding medium of equivalent homogeneous material. Different points in this approach are confusing but the most difficult to accept is the as-

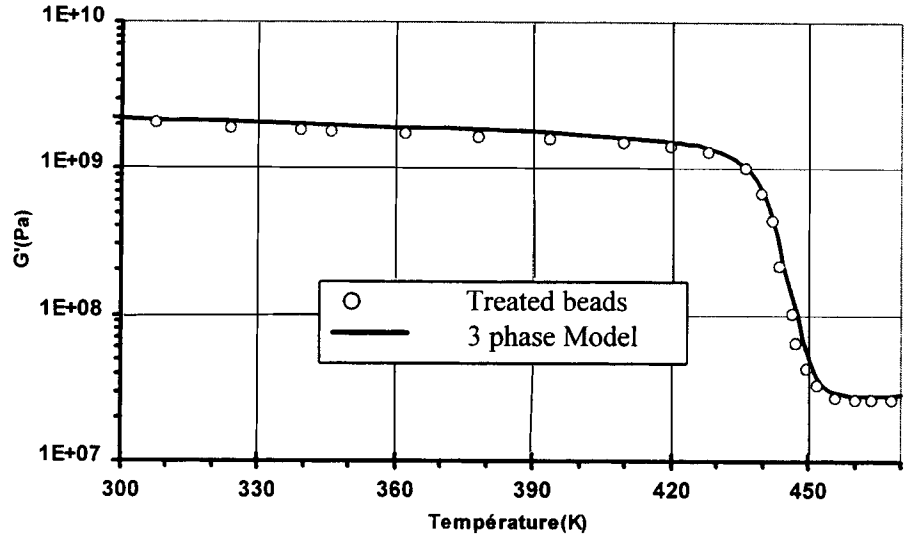


Fig. 6. Experimental data compared with calculated results (3-phase model applied in one step) for the composite 30%: untreated and treated glass beads.

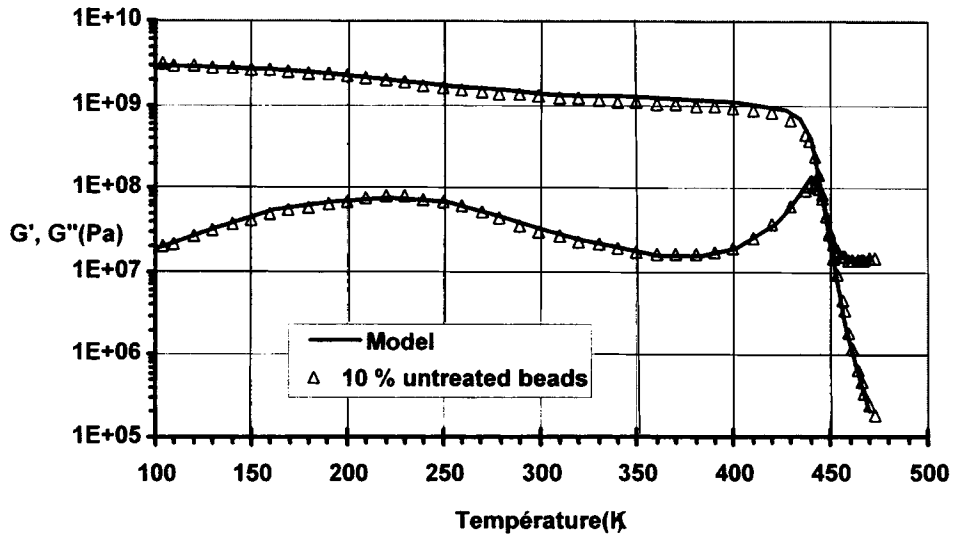
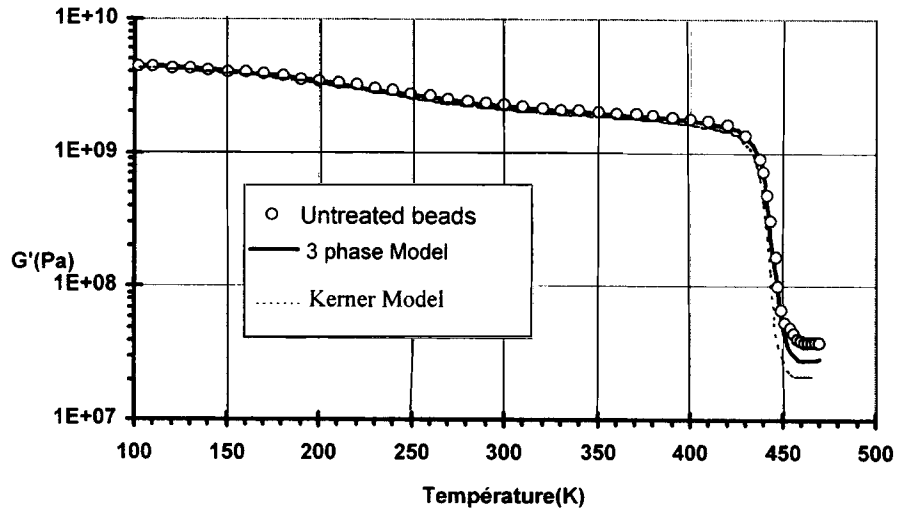
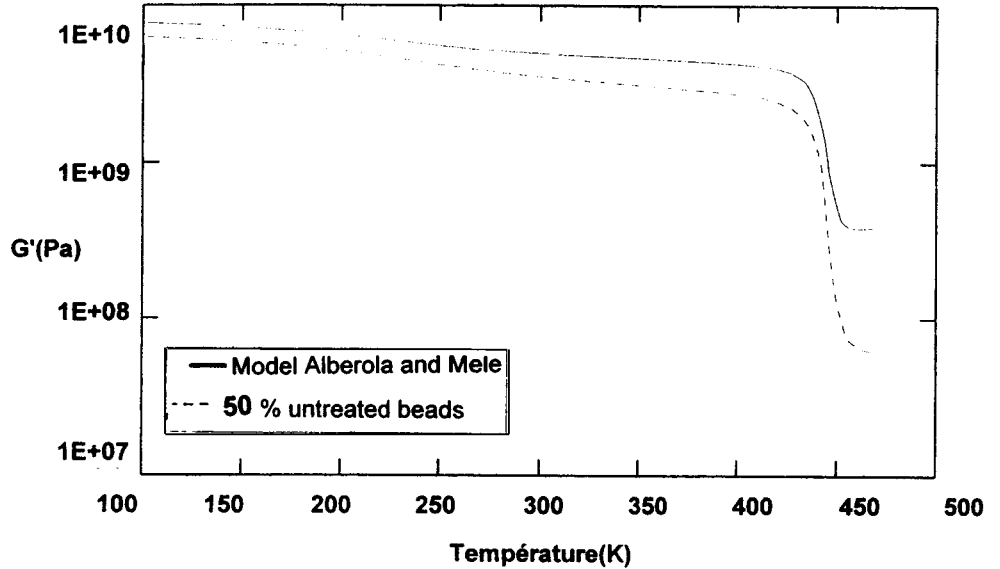


Fig. 7. Experimental data compared to calculated results (3-phase model applied in one step) for the composite 10%: untreated glass beads.

Fig. 8. Experimental data compared with calculated results (Mele and Alberola's 4-phase model) for the composite with 50% untreated glass beads.



sumption of glass continuity as far as beads are concerned. In any case, this model fails to fit the rubbery modulus as illustrated in Fig. 8 for a glass volume fraction of 50%. Nevertheless, according to the percolation theory, the existence of aggregates of a finite size is no doubt below the percolation threshold. But, the nonhomogeneous distribution of the filler is an important parameter that is not correctly taken into account in the Mele and Alberola approach since the modulus of an aggregate cannot be so high as the one of the glass. Thus, in the following section, we propose to use the 3-phase model in successive steps in order to account for the nonhomogeneous distribution of the filler.

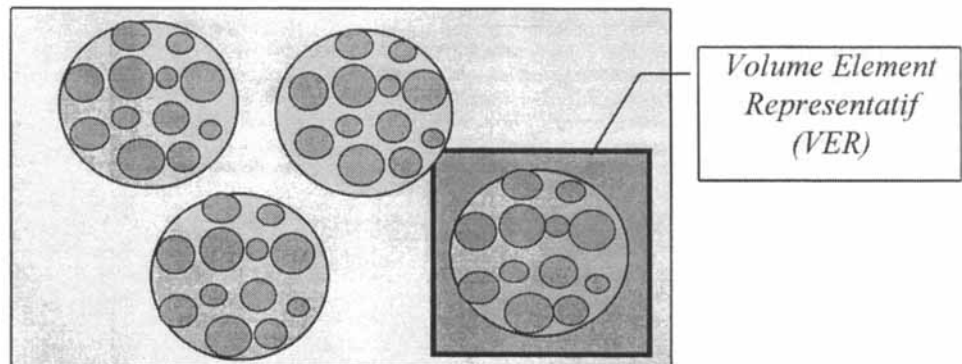
### 5.3 Two Successive Steps—Application of the 3-Phase Model

More accuracy can then be expected from a better description of the observed phase organization. In other words, the composite material can be regarded as a matrix reinforced by spherical inclusions, being themselves composite systems with a volume fraction

of glass spheres higher than the nominal one (Fig. 9). Considering that the morphology is described using different scales of heterogeneity, we decided to use the 3-phase model in two successive applications. Such a successive application of the analytical micromechanical model has already been proposed in the literature in the case of metallic materials (29, 30) and also for unidirectional composites (16).

In the first step (Fig. 10a), the properties of highly filled zones, i.e., for which the glass beads are agglomerated (*Highly Reinforced Zones*) were calculated with three components; (i) the spherical inclusion with a volume fraction  $\phi_{hrz}$  higher than the mean value; (ii) a shell based on the polymer matrix; (iii) a surrounding medium of equivalent homogeneous material. In the second step (Fig. 10b), the three components considered for the calculation are: (i) the highly filled zone as a spherical inclusion (thus, considered as a new type of inclusion), having the properties calculated in the first step; (ii) a matrix shell; and (iii) the surrounding region of equivalent homogeneous media with infinite dimensions. Note that the maximum volumetric packing fraction of spheres is de-

Fig. 9. Scheme of the spherical composite inclusions (highly reinforced zones).



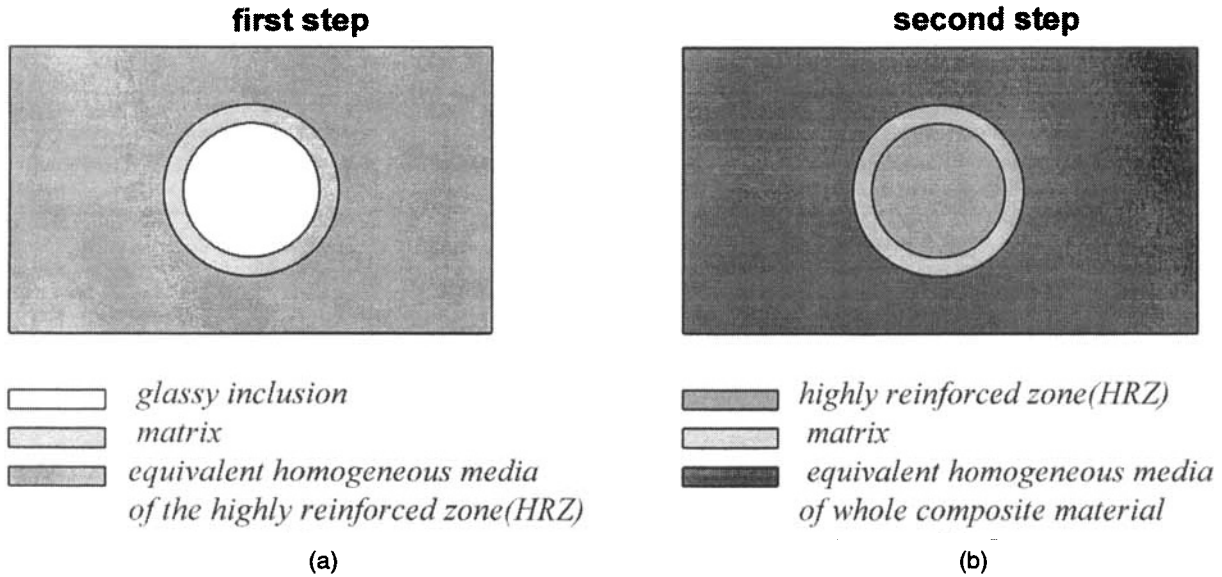


Fig. 10. Three-phase model of solution in the two steps of calculation.

scribed as random close packing, with the value of the  $\phi_{max} = 0.68$  (27, 28).

This model requires that the effective homogeneous medium have the same average conditions of stress and strain as for the spherical model described in Fig. 5. In this two-step analysis, the Poisson's coefficient is considered temperature dependent (Eq 8). Actually, the value of  $\phi_{hrz}$  can be used as a fitting parameter. However, it can be estimated from morphological studies while it corresponds to the volume fraction of glass beads in the highly reinforced zones. It appears that the  $\phi_{hrz}$  parameter goes through an optimum value to give the best fit for composites based on 30 vol% of glass, equal to 51% (Fig. 11). The fitted curves for a composite based on 50% of glass using  $\phi_{hrz}$  as 64% is presented in Fig. 12. Table 2 shows the best

calculated fittings of the dynamic mechanical properties of composite material based on different untreated glass bead contents.

To sum up, these results show that the morphology of the composite material plays an important role for the dynamic mechanical behavior of particulate composites. Of course, the two successive applications is somehow schematic while it represents all the agglomerates as ideal spheres. Nevertheless, it already gives a rough description of the morphology, leading to an accurate estimation of the whole set of experimental data, i.e.,  $G'$ ,  $G''$ , and  $\tan\phi$  versus temperature. Moreover, from the mechanical analysis of the data, we can conclude that there are differences in the bead distribution in the two samples: surface treatment leads to a more homogeneous state of distribution in the mate-

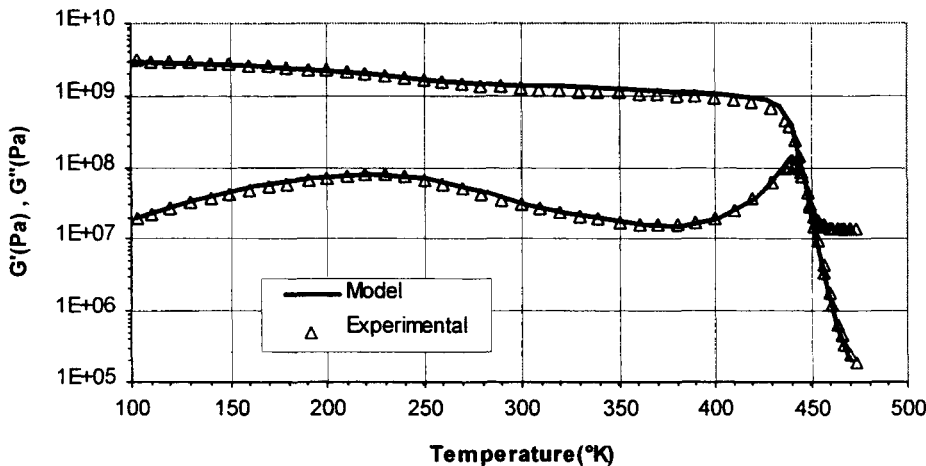


Fig. 11. Experimental data compared with calculated results (3-phase model applied in two successive steps) for the composite based on 30 vol% of untreated glass beads:  $\phi_{hrz} = 51\%$ .

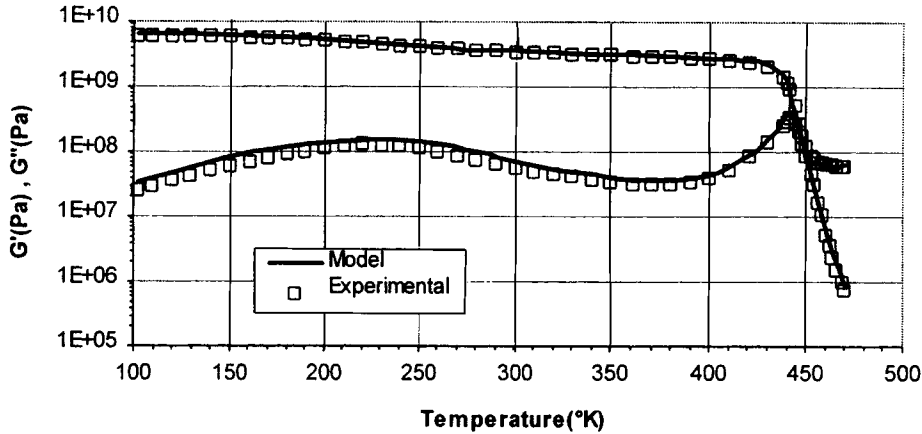


Fig. 12. Experimental data compared to calculated results (3-phase model applied in two successive steps) for the composite based on 50 vol% of untreated glass beads:  $\phi_{fuz} = 65\%$ .

rial. That point is consistent with the influence of the sizing on the surface energy of the beads.

**6. CONCLUSION**

In this work, the “generalized self-consistent” 3-phase model is used to predict the dynamic mechanical behavior of composite materials based on epoxy and glass beads. When the distribution of the filler is more or less homogeneous, the direct application of the 3-phase model gives an accurate estimation. On the contrary, with a heterogeneous distribution of beads, it is necessary to take into account this specific morphology of the composite material, by using the 3-phase model in two successive steps. This route appears to give better estimates than calculations obtained from other related models based on the 4-phase formulations proposed in the literature.

We can conclude that the knowledge of the spatial distribution of filler in the composites material is one of the important parameters for modeling this dynamic mechanical behavior. Moreover, this work actually indicates that no coupling model is universal. The best accuracy can then be expected from a good description of the observed phase organization. In order to validate this approach, it could be very interesting to analyze quantitatively the distribution of glass beads in the composite sample. In order to obtain 3-dimensional in-

formation, the study of the morphology of both samples (with, resp., treated and untreated beads) is at this moment carried out by RX tomography.

**APPENDIX**

The final solution from Herve and Zaoui for  $G^*$  of the particulate composite is given by the results of the quadratic equation (Eq A-1):

$$X \left( \frac{G_c^*}{G_m^*} \right)^2 + Y \left( \frac{G_c^*}{G_m^*} \right) + Z = 0 \tag{A-1}$$

where, X, Y, and Z are constants. For the 3-phase model, the following simplified expressions are:

$$X = 4R_2^{10} (1 - 2\nu_m) (7 - 10\nu_m) H_{12} + 20R_2^7 (7 - 12\nu_m + 8\nu_m^2) H_{42} + 12R_2^5 (1 - 2\nu_m) \times (H_{14} - 7H_{23}) + 20R_2^3 (1 - 2\nu_m)^2 H_{13} + 16 (4 - 5\nu_m) (1 - 2\nu_m) H_{43} \tag{A-2}$$

$$Y = 3R_2^{10} (1 - 2\nu_m) (15\nu_m - 7) H_{12} + 60R_2^7 (\nu_m - 3)\nu_m H_{42} - 24R_2^5 (1 - 2\nu_m) \times (H_{14} - 7H_{23}) - 40R_2^3 (1 - 2\nu_m)^2 H_{13} - 8 (1 - 5\nu_m) (1 - 2\nu_m) H_{43} \tag{A-3}$$

$$Z = -R_2^{10} (1 - 2\nu_m) (7 + 5\nu_m) H_{12} + 10R_2^7 (7 - \nu_m^2) H_{42} + 12R_2^5 (1 - 2\nu_m) \times (H_{14} - 7H_{23}) + 20R_2^3 (1 - 2\nu_m)^2 H_{13} - 8 (7 - 5\nu_m) (1 - 2\nu_m) H_{43} \tag{A-4}$$

where  $R_2 = 1$  and  $H_{\eta\beta}$  are the products of the members of the following matrix P, and thus  $\eta(\beta)$  are the numbers of line (column) of the matrix H:

$$H_{12} = P_{1,1} \cdot P_{2,2} - P_{2,1} \cdot P_{1,2}$$

$$H_{13} = P_{1,1} \cdot P_{3,2} - P_{3,1} \cdot P_{1,2}$$

$$H_{14} = P_{1,1} \cdot P_{4,2} - P_{4,1} \cdot P_{1,2}$$

$$H_{23} = P_{2,1} \cdot P_{3,2} - P_{3,1} \cdot P_{2,2}$$

$$H_{42} = P_{4,1} \cdot P_{2,2} - P_{2,1} \cdot P_{4,2}$$

$$H_{43} = P_{4,1} \cdot P_{3,2} - P_{3,1} \cdot P_{4,2}$$

**Table 2. Calculated Optimized Characteristics, for Composites Based on the Volume Fraction of Untreated Glass Beads.**

	T $\alpha$ (K)	tan( $\delta$ ) <sub>max</sub>	G'(MPa) (at T=100K)	G'(MPa) (at T=464K)
Composite 10%	446	1.08	2990	14.3
Composite 20%	447	1.006	3700	20.1
Composite 30%	448	0.989	4450	39.2
Composite 50%	448	0.985	6610	64.2

with matrix of P:

$$P = \frac{1}{5(1 - \nu_m)} \begin{bmatrix} \frac{c}{3} & \frac{R_1^2(3b - 7c)}{5(1 - 2\nu_f)} & \frac{-12\alpha}{R_1^5} & \frac{4(f - 27\alpha)}{15(1 - 2\nu_f)R_1^3} \\ 0 & \frac{(1 - 2\nu_m)b}{7(1 - 2\nu_f)} & \frac{-20(1 - 2\nu_m)\alpha}{7R_1^7} & \frac{-12\alpha(1 - 2\nu_m)}{7(1 - 2\nu_f)R_1^5} \\ \frac{R_1^5\alpha}{2} & \frac{-R_1^7(2a + 147\alpha)}{70(1 - 2\nu_f)} & \frac{d}{7} & \frac{R_1^2[105(1 - \nu_m) + 12\alpha(7 - 10\nu_m) - 7e]}{35(1 - 2\nu_f)} \\ -\frac{5}{6}(1 - 2\nu_m)\alpha R_1^3 & \frac{7(1 - 2\nu_m)\alpha R_1^5}{2(1 - 2\nu_f)} & 0 & \frac{e(1 - 2\nu_m)}{3(1 - 2\nu_f)} \end{bmatrix}$$

with:

$$a = \left(\frac{G_f^*}{G_m^*}\right) \cdot (7 + 5\nu_f) \cdot (7 - 10\nu_m) - (7 - 10\nu_f) \cdot (7 + 5\nu_m)$$

$$b = 4(7 - 10\nu_f) + \left(\frac{G_f^*}{G_m^*}\right) \cdot (7 + 5\nu_f)$$

$$c = (7 - 10\nu_m) + 2\left(\frac{G_f^*}{G_m^*}\right) \cdot (4 - 5\nu_m)$$

$$d = (7 + 5\nu_m) + 4\left(\frac{G_f^*}{G_m^*}\right) \cdot (7 - 10\nu_m)$$

$$e = 2(4 - 5\nu_f) + \left(\frac{G_f^*}{G_m^*}\right) \cdot (7 - 5\nu_f)$$

$$f = (4 - 5\nu_f) \cdot (7 - 5\nu_m) - \left(\frac{G_f^*}{G_m^*}\right) \cdot (4 - 5\nu_m) \cdot (7 - 5\nu_f)$$

$$\alpha = \left(\frac{G_f^*}{G_m^*}\right) - 1$$

**NOMENCLATURE**

- $G_c^*, G_c', G_c''$  Complex, storage, and loss moduli of the composite.
- $G_m^*, G_m', G_m''$  Complex, storage, and loss moduli of the matrix.
- $G_f$  Shear modulus of the glass beads.
- $E$  Young's modulus.
- $\nu_m, \nu_f$  Poisson's coefficients of the matrix and the filler, respectively.
- $\tan\delta$  Loss factor ( $G''/G'$ ).
- $T_g$  Glass transition temperature.
- $R_1, R_2, R_3$  Radii of the spherical inclusion, the surrounding matrix, and the equivalent homogeneous media, respectively.
- $r, \theta, \gamma$  Spherical coordinates.
- $U_r, U_\theta, U_\gamma$  Displacement components in the  $r, \theta,$  and  $\gamma$  directions.

- 1, 2, 3 Subscripts referring to spherical inclusion, matrix, and equivalent homogeneous surrounding media, respectively.
- $\phi_f, \phi_m$  Volume fraction of the filler and the matrix, respectively.
- $\phi_{max}$  Maximum volume packing fraction.
- $\phi_{hrz}$  Volume fraction of the highly reinforced zones.
- VER Volume element representative.
- DGEBA Diglycidyl ether of bisphenol-A.
- IPD Isophorone diamine.
- HRZ Highly reinforced zones.

**REFERENCES**

1. T. B. Lewis and L. E. Nielsen, *J. Appl. Polym. Sci.*, **14**, 1449 (1970).
2. A. E. Nielsen and R. F. Landel, in *Mechanical Properties of Polymers and Composites*, Dekker, New York (1994).
3. R. M. Christensen, *Theory of Viscoelasticity*, Academic Press, New York (1971).
4. Takayanagi, K. Imada and T. Kajiyama, *J. Polym. Sci.: Part C*, **15**, 263 (1966).
5. Z. Hashin and S. Shtrikman, *J. Mech. Phys. Solids*, **11**, 127 (1963).
6. R. Hill, *J. Mech. Phys. Solids*, **13**, 213 (1965).
7. B. Budiansky, *J. Mech. Phys. Solids*, **13**, 223 (1965).
8. E. H. Kerner, *Proc. Roy. Soc. Lond.*, **69B**, 808 (1956).
9. R. M. Christensen and K. H. Lo, *J. Mech. Phys. Solids*, **27**, 315 (1979). Erratum: **34**, 639 (1986).
10. F. H. J. Maurer, *Elsevier Sci. Co.*, Ishida, ed., 491 (1990).
11. N. Alberola and P. Mele, *Polym. Compos.*, **17**, 751 (1996).
12. E. Herve and A. Zaoui, *Eur. J. Mech. A/Solids*, **9**(6), 505 (1990).
13. H. A. Waterman, *Kolloid Z. Z. Polym.*, **192**, 1 (1963).
14. A. Agbossou, A. Bergeret, K. Benzarti, and N. Alberola, *J. Mater. Sci.*, **28**, 1963 (1993).
15. A. F. Yee, and M. T. Takemori, *J. Polym. Phys.*, **20**, 205 (1982).
16. C. Gauthier, A. Khavandi, P. Franciosi, R. Gaertner, and J. Perez, *J. Polym. Compos.*, accepted (1997).
17. Y. G. Won, PhD thesis, 20, INSA, Lyon, France (1989).
18. J. Y. Cavaille, M. Salvia, and P. Merzeau, *Spectre 2000*, **16**, 37 (1988).
19. V. B. Gupta, L. T. Drzal, and C. Y-C. Lee, *Polym. Eng. Sci.*, **25**, 812 (1985).
20. P. H. Dederichs and R. Z. Zeller, *Z. Phys.*, **259** 103 (1973).
21. E. Kroner, *J. Mech. Phys. Solids*, **25**, 137 (1977).

22. Z. Hashin, *J. Applied Mechanics*, **29**, 143 (1962).
23. J. K. Mackenzie, *Proc. Roy. Soc.*, **63**, 2 (1950).
24. A. E. H. Love, in *A Treatise on the Mathematical Theory of Elasticity*, Dover, New York (1944).
25. Z. Hashin, *J. Solids Structures*, **6**, 539 (1970).
26. Z. Hashin, *J. Solids Structures*, **6**, 797 (1970).
27. G. D. Scott, *Nature*, **188**, 908 (1960).
28. R. K. McGeary, *J. Amer. Ceram. Soc.*, **44**, 513 (1961).
29. E. Maire, D. S. Wilkinson, J. D. Embury, and R. Fougères *Acta Materialia*, **65**, 5261 (1997).
30. S. F. Corbin and D. S. Wilkinson, *Acta Metall. Mater.*, **42**, 1311 (1994).